Int. J. Electrochem. Sci., 11 **(2016)** 5631 – 5654, doi: 10.20964/2016.07.17

International Journal of
ELECTROCHEMICAL
SCIENCE
www.electrochemsci.org

Wear and Corrosion Performance of PEO-synthesized SiC Nanocomposite Coatings: Effect of Processing Time and Current Density

H. Nasiri Vatan, R. Ebrahimi-Kahrizsangi[*]*, M. Kasiri-Asgarani*

Advanced Materials Research Center, Materials Engineering Department, Islamic Azad University, Najafabad Branch, Najafabad, Isfahan, Iran
[*]E-mail: rezaebrahimi@iaun.ac.ir

Received: 8 March 2016 / *Accepted:* 29 April 2016 / *Published:* 4 June 2016

In the present study, a systematic investigation of the effect of the process parameters on the final properties of the PEO coatings was done. Protective oxide coatings were prepared on AZ31 magnesium alloy by plasma electrolytic oxidation (PEO) process using aluminate-silicate based electrolyte containing SiC nanoparticles in different current densities and time intervals. Microstructural characterization of the PEO treated samples was evaluated by scanning electron microscopy (SEM) followed by image analysis and energy dispersive spectroscopy (EDS). Wear resistance of the coatings was analyzed by ball-on disc tribometer. The corrosion resistance of the coatings was also investigated with potentiodynamic polarization and electrochemical impedance spectroscopy (EIS) tests in 3.5 wt.% NaCl solution. It was found that the processing time and current density have a significant influence on the resulting coatings properties, such as microstructure, thickness, composition, hardness, wear and corrosion behavior. The thick coatings produced at higher current density and treatment time possess a high hardness and provide a low friction coefficient and wear rate against stainless steel balls. They also improved the corrosion resistance compared with the uncoated magnesium alloy, which can be mainly due to their compactness, thickness and microstructure.

Keywords: Magnesium; Plasma Electrolytic Oxidation; Wear; Corrosion

1. INTRODUCTION

Magnesium and its alloys have low density, high strength to weight ratio, good dimensional stability and good electromagnetic shielding properties, which are very attractive to a wide range of industries, especially in automotive, aerospace, electronics and biomedical sectors [1,2].

Unfortunately, magnesium and its alloys exhibit a very poor corrosion resistance. This disadvantage is primarily due to their high chemical activity and also to the unstable natural oxide film on their surfaces, and has limited their widespread use in many applications [3]. Another main factor limiting the application of Mg alloys is their comparatively low wear resistance [4].

Surface modification in the form of an oxide coating on the magnesium alloy substrate is one of the most effective ways to prevent wear and corrosion. So far, numerous surface treatments have been used to provide corrosion protection for magnesium and its alloys which include phosphating, chromating, plating, organic coating, gas-phase deposition processes, anodization, etc. [5]. Among them, plasma electrolytic oxidation (PEO) has been known as a promising surface treatment for light weight metals (especially aluminum, magnesium, titanium and their alloys) to improve the electrochemical and tribological properties of the alloys via producing a relatively thick and dense coating [6]. PEO method has some advantages over the other surface treatments including excellent adhesion of the oxide coating to the substrate, single-step processing, relatively low cost, ease of controlling and environmentally friendly processing [7,8]. These characteristic of the PEO coatings are mainly dependent on the process parameters, chemical composition of the substrate and the electrolyte used [9].

The electrolyte composition, electrical parameters, additives, temperature, and substrate material all affect the coating surface morphology, composition, and wear and corrosion resistance [10,11]. Among different forms of PEO process, the DC PEO mode is the easiest and most convenient to investigate the fundamental aspects of the oxide coating formation process in relation to the basic process parameters [12]. However, so far, there is only limited data about the effect of treatment time and current density in the nanoparticle-containing electrolyte on the structural and final properties of the PEO coatings formed on magnesium alloy.

In this study, the oxide layers incorporated with SiC nanoparticles were successfully produced, and their structural, tribological and electrochemical characteristics were evaluated using SEM, wear and corrosion tests. Furthermore, the effects of treatment time and current density on the above-mentioned properties, and also the growth mechanisms of oxide layers fabricated in electrolytes with and without SiC nanoparticles were elucidated.

2. EXPERIMENTAL PROCEDURE

2.1 Materials

The substrate used in this study was AZ31 Mg alloy. Rectangular specimens with dimensions of 2 cm × 2 cm × 1 cm were prepared from Mg sheet. Prior to PEO treatment, the samples were mechanically ground with silicon carbide emery papers (up to 1000 grit); rinsed with water, then degreased in ethanol and finally dried with hot air.

2.2. Preparation of the electrolyte and PEO process

PEO treatment was performed under constant current densities of 11.5 and 23 mA/cm^2 at 30 °C with a 20 kW power supply using a glassy-vessel container as an electrolyte cell. A cylindrical coil made of stainless steel pipe was used as cathode and also as cooling system in the PEO process. Samples were subjected to the PEO process with an applied current density of 11.5 and 23 mA/cm^2 for different time intervals (i.e. 5, 10, 15 and 20 min) in an electrolyte consisting of 2 g/L sodium aluminate ($NaAlO_2$, Aldrich), 2 g/L sodium metasilicate (Na_2SiO_3, Aldrich) and 1.5 g/L potassium hydroxide (KOH, Merck). SiC fine nanoparticle was received from Plasmachem (Germany) with the average particle size of about 30 nm (Fig.1) and was added to the electrolyte (5 g/lit).

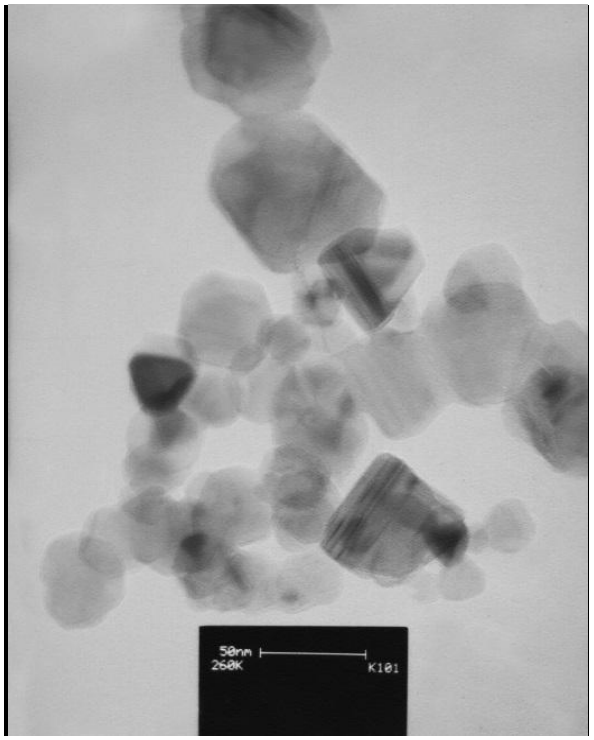

Figure 1. TEM image of the SiC nanoparticles.

After the PEO treatment, the samples were rinsed in ethanol and distilled water, and then dried in air at room temperature.

2.3. Characterization of the coatings

2.3.1. Microstructure examination

The surface morphology and cross-section of the PEO coatings were observed using a scanning electron microscope (SEM, SIGMA/VP). The compositional analysis of the oxide layers was investigated with energy dispersive spectrometer (EDS) attached to the SEM. Surface porosity and average diameters of the pores of the oxide layers was measured based on the SEM micrographs.

2.3.2. Micro-hardness and wear measurements

The microhardness of the oxide coatings was measured by means of an MH-5 hardness tester with a Vickers indenter at a load of 10 g and for a loading duration time of 5 s. The friction and wear characteristics of the PEO-synthesized coatings were evaluated in a ball-on-disc configuration against stainless steel balls of Ø 3 mm using a reciprocal-sliding UMT-2MT tribometer under dry sliding conditions. Wear rates (ω) of the coatings can be calculated from the following equation:

$$\omega = \frac{V}{(L \times N)} \qquad \text{Eq.1}$$

Where, V is wear volume, L is sliding distance and N is load.

2.3.3. Electrochemical measurements

The electrochemical behavior of the samples was examined using Solarton 1250 potentiostat and a conventional three-electrode cell, employing a saturated calomel electrode (SCE) as the reference electrode and a platinum grid as the counter electrode. The PEO-coated samples were used as the working electrode, the test solution was 3.5 wt.% NaCl, and all of the corrosion tests were carried out at room temperature. After 10 minutes of immersion in NaCl solution (to reach a relatively stable condition), electrochemical impedance spectroscopy (EIS) measurements were conducted with a frequency range of 10mHz-1MHz and a 10 mV peak-to-peak AC excitation. In the Potentiodynamic polarization tests were conducted at a scan rate of 1 mV/s from -0.30 V to +1.0 V with respect to open circuit potential.

3. RESULTS AND DISCUSSION

3.1. Voltage-time curves for PEO treatment

Voltage-time behaviors of the AZ31 Mg alloy in the aluminate-silicate electrolyte with and without SiC nanoparticles in different current densities are represented in Fig.2. These curves can be characterized by four stages in both electrolytes.

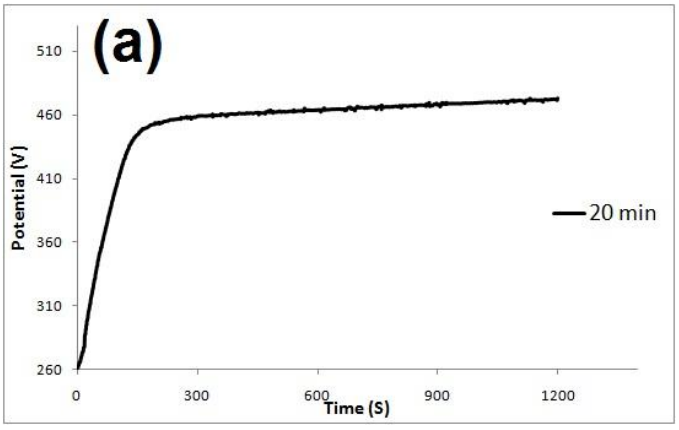

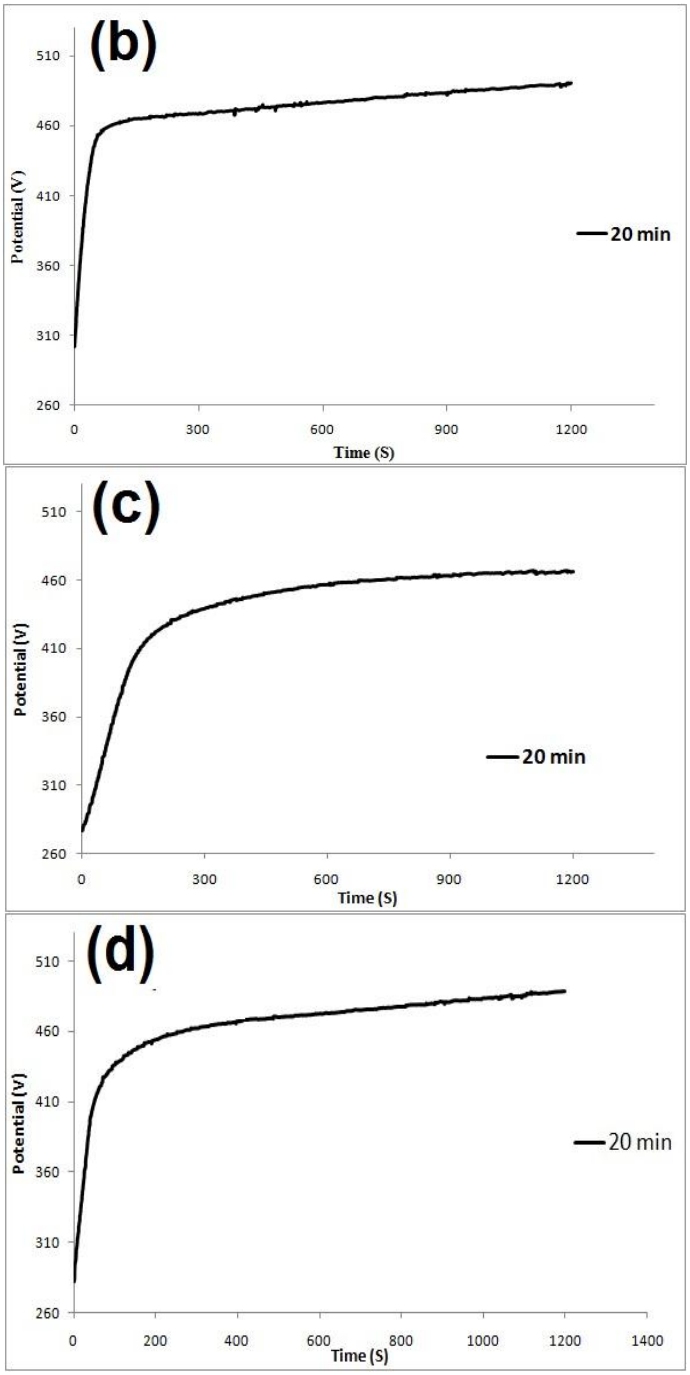

Figure 2. Voltage-time responses for PEO process of AZ31 Mg alloy substrate in alkaline aluminate-silicate electrolyte in the absence (a,b) and presence (c,d) of SiC nanoparticles in current densities of 11.5 (a,c) and 23 mA/cm^2 (b,d).

During the first stage (50-60 s), the dissolution of the substrate is accompanied by the formation of a thin barrier layer on the surface of the substrate, and the voltage increases linearly with time in a constant rate. In this stage, no apparent sparks were found on the substrate surface. When the voltage reaches a critical value, sparking occurs. The critical voltage, defined as the breakdown voltage, is responsible for the formation of micro sparks on the surface of the sample and has a strong dependence on the electrolyte composition and conductivity [13,14]. In this stage (stage II), a large

number of uniformly distributed small sparks were appeared on the sample surface. The rate of increase of voltage during the second stage decreases in both electrolytes. In the third stage, the lifetime and size of the micro sparks on the surface of the sample increase, and the slope of the curve becomes smaller than the second stage. Then, the process enters the stage four and a relatively steady voltage was established on the sample surface. In the fourth stage, the appearance of the micro sparks was gradually changed; their population decreased but their size and lifetime increase, their color was also changed from white to orange and red. The final voltage of V-t curves of the samples treated in the alkaline aluminate-silicate electrolyte at current density of 23 mA/cm^2 are relatively higher than those processed at lower current density. Visual observations during the PEO process confirmed that the discharges become steadier in the higher current density, which is in good agreement with previous investigations [15]. The voltage responses during the PEO process were practically the same in the electrolyte without and with SiC nanoparticles. This means that the addition of SiC nanoparticles did not significantly affect the variation of oxidation potential during the PEO process.

3.2. Structural properties

Surface morphologies of the coatings produced in SiC-free electrolyte under different current densities and processing times are shown in Fig.3.

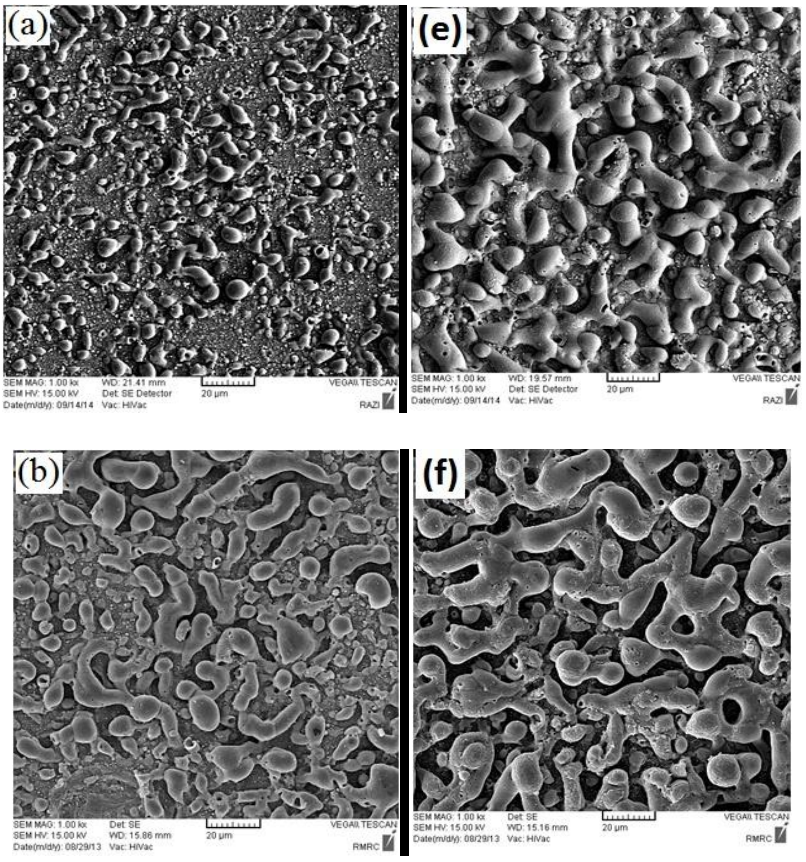

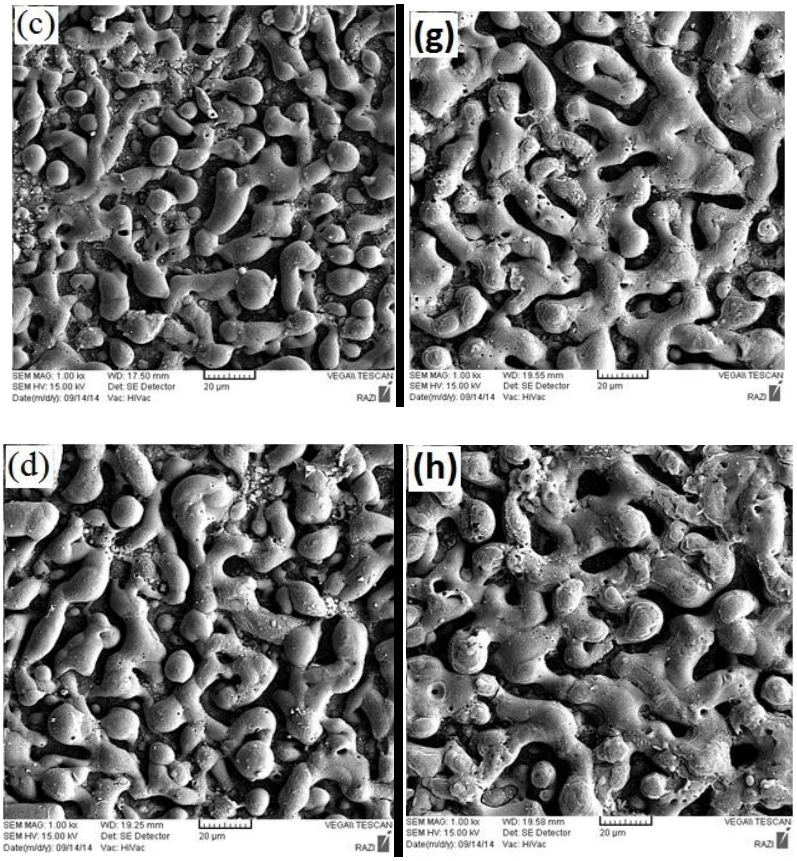

Figure 3. SEM surface morphology of the PEO coatings grown in SiC-free electrolyte under different conditions: current density of 11.5 mA/cm^2 (a) 5, (b) 10, (c) 15 and (d) 20 min; current density of 23 mA/cm^2 (e) 5, (f) 10, (g) 15 and (h) 20 min.

As can be seen, the PEO films have relatively high porosity and some microcracks on the surface. It has been verified that the formation of the pores is mainly due to the molten oxide and gas bubbles thrown out of the discharge channels. The appearance of the repeated and concentrated sintering on the surface of the oxide coatings may be related to the characteristics of the micro-sparks during the PEO process [16]. The SEM micrographs of the coatings suggest outward flow of material along a discharge channel through the underlying coating to the coating surface, and then spreading over the coating surface and solidification [17]. The surface of the coatings is rough, and many pores and cracks are evident. Furthermore, a great influence of the treatment time and current density is visible in the surface morphology of the produced coatings. There is an increasing amount of porosity on the surface with increasing of treatment time and current density. Liang et al. [18] and Li et al. [19] studied the effect of applied current density on the properties of PEO coatings on magnesium alloy and found that higher current densities result in intensified sparking discharges, which in turn lead to enlarged pore size on the surface of the coatings. It is also observed that the pore size increases with treatment time. Bayati et al. [19,20] showed that when a structural defect (such as pore) forms by an electrical discharge, it is a more susceptible place for next electron avalanches because of its lower breakdown voltage in comparison with other areas of the surface which are not porous [21].

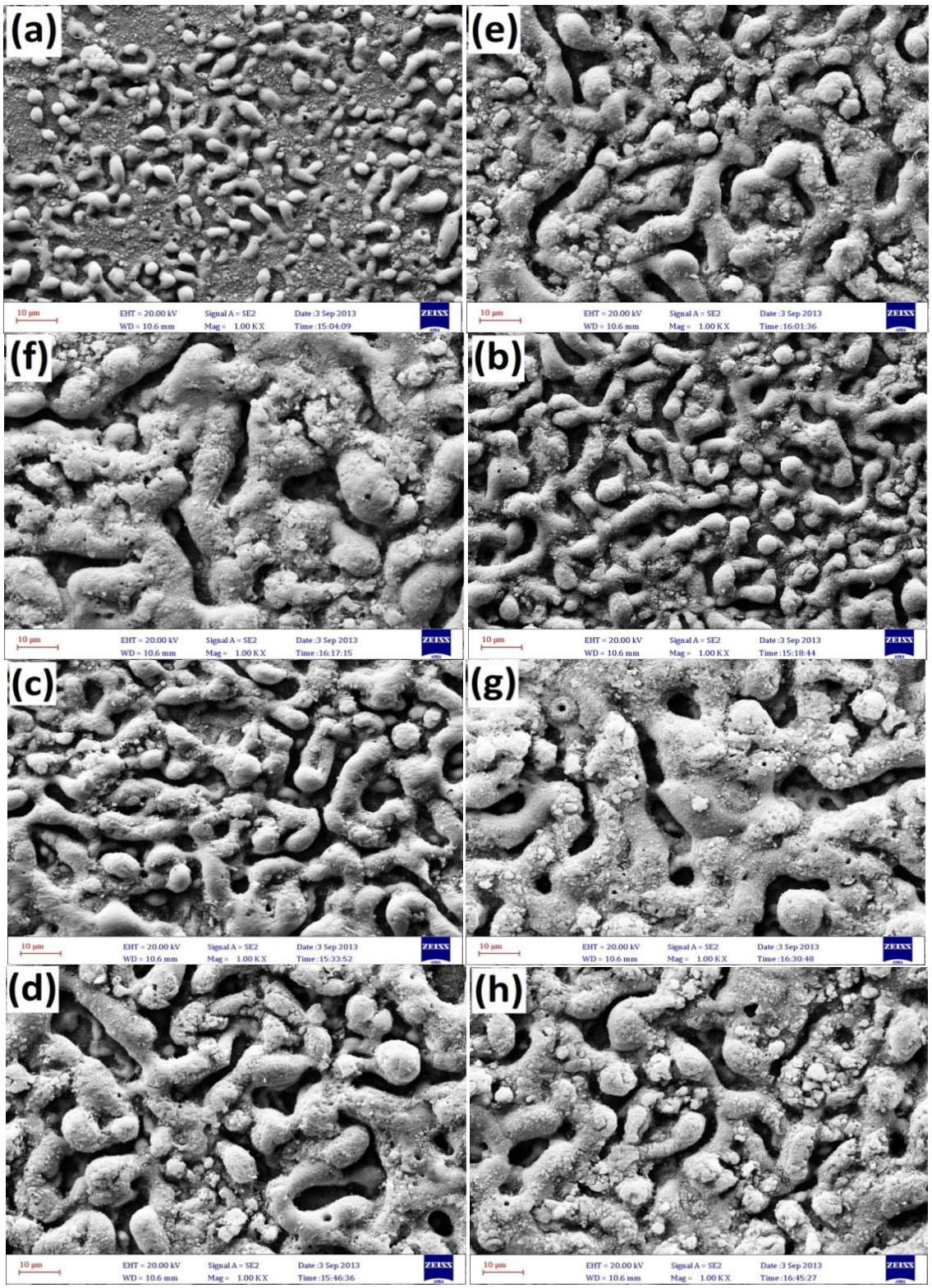

Figure 4. SEM surface morphology of the PEO coatings grown in SiC-containing electrolyte under different conditions: current density of 11.5 mA/cm^2 (a) 5, (b) 10, (c) 15 and (d) 20 min; current density of 23 mA/cm^2 (e) 5, (f) 10, (g) 15 and (h) 20 min.

Fig.4 shows the surface morphologies of the PEO coatings on AZ31 magnesium alloy with SiC nanoparticles. The results show that the pore size and porosity remained relatively constant,

irrespective of the presence of SiC nanoparticles in the electrolyte. It can be due to this fact that the pore size and porosity are mainly dependent on the electrical conductivity and pH of the electrolyte [22,23], whose values in the absence and presence of SiC nanoparticles were almost similar. However, many nanoparticles can be observed on the surface of the PEO coatings obtained in SiC-containing electrolyte. It is also seen that the density of the SiC nanoparticles on the surface increases with the treatment time and current density. The reason is that with increasing the current density and treatment time the voltage of the process is also increases, which intensifies the electric field between the anode and cathode and hence more SiC nanoparticles are moved towards the substrate to participate in the reactions.

Cross-sectional SEM images of the PEO coatings formed in the electrolyte without and with SiC nanoparticles are shown in Figs.5 and 6, respectively.

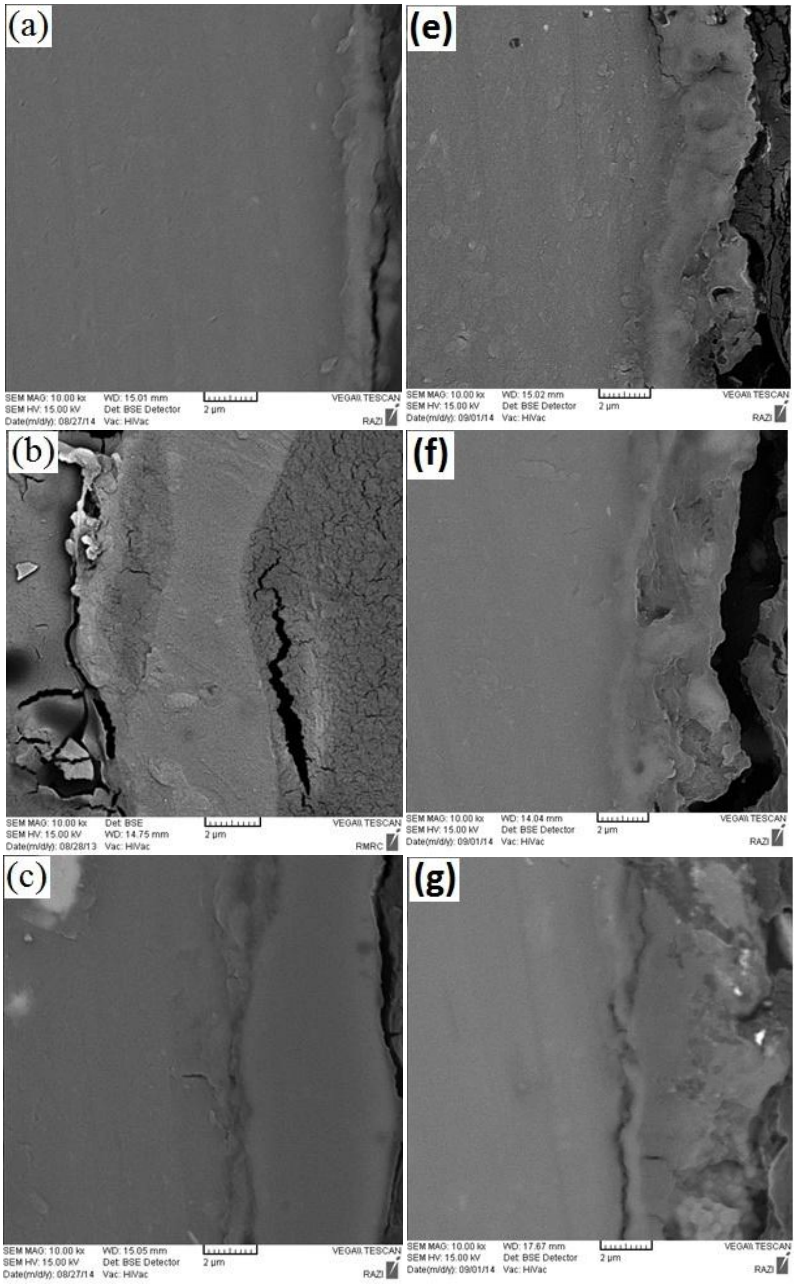

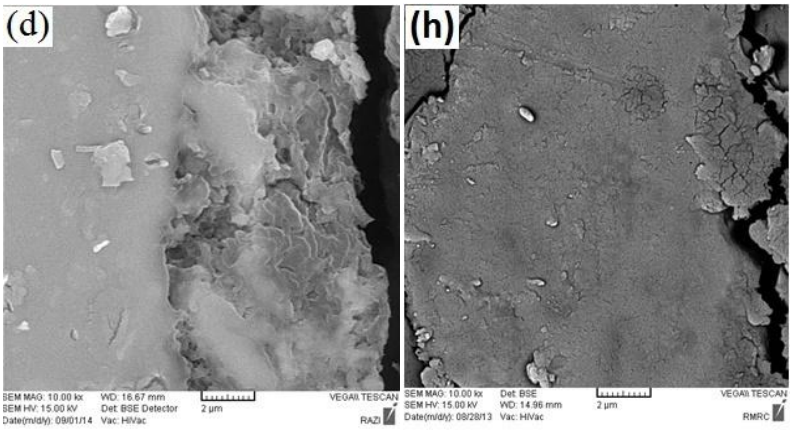

Figure 5. SEM micrographs (backscattered electrons) of cross-section of AZ31 magnesium alloy after PEO treatment in SiC-free electrolyte in current density of 11.5 mA/cm^2 (a-d) and 23 mA/cm^2 (e-h) for 5 min (a,e), 10 min (b,f), 15 min (c,g) and 20 min (d,h).

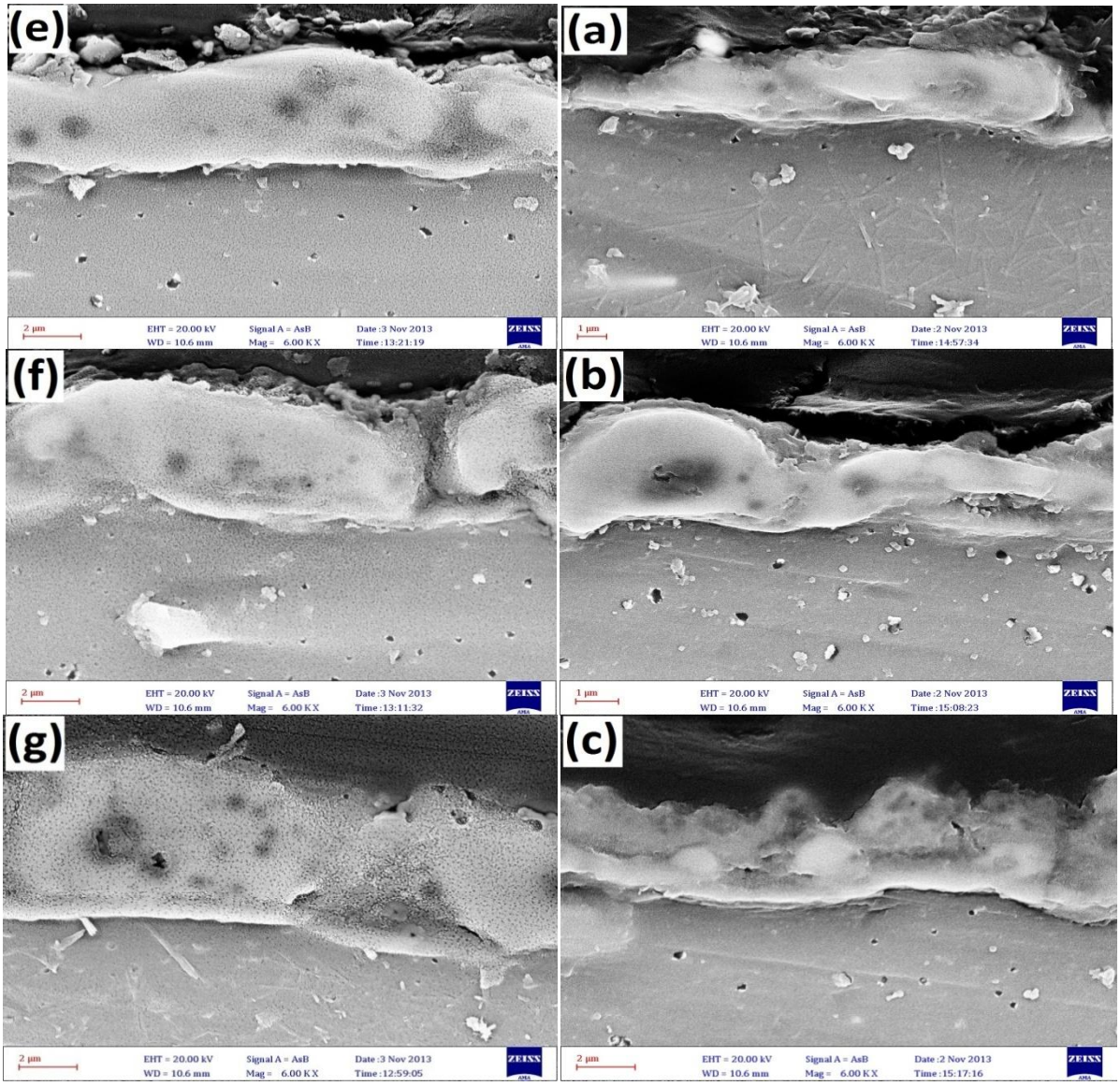

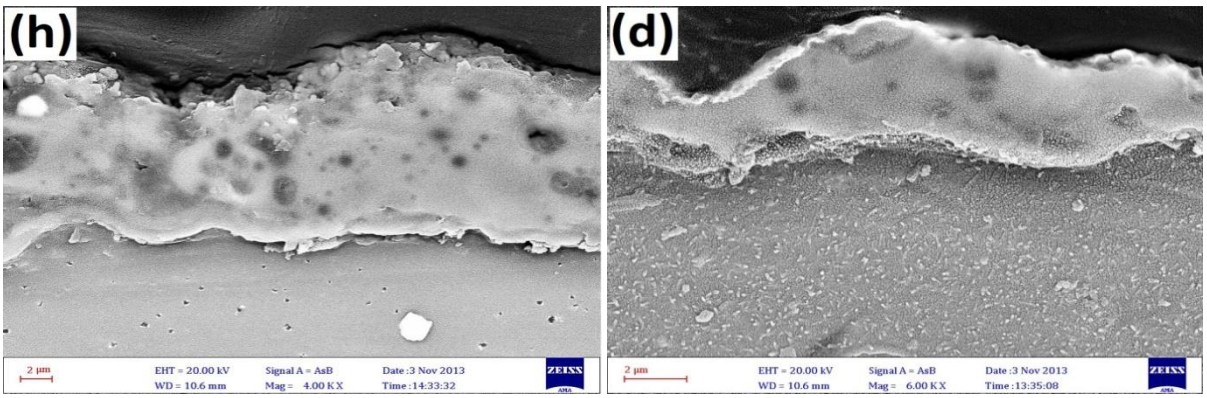

Figure 6. SEM micrographs (backscattered electrons) of cross-section of AZ31 magnesium alloy after PEO treatment in SiC-containing electrolyte in current density of 11.5 mA/cm^2 (a-d) and 23 mA/cm^2 (e-h) for 5 min (a,e), 10 min (b,f), 15 min (c,g) and 20 min (d,h).

No matter if SiC nanoparticles were added or not, SEM images of the cross-sections of the oxide layers disclose that the coatings contain relatively large pores and the thickness of the oxide coatings is not homogeneous. The thickness of the PEO coatings obtained from electrolytes with and without SiC nanoparticles is relatively the same, which is consistent with the results of the literature [24]. As can be seen, the average thickness of the coatings increases as the applied current density increases. Investigations have demonstrated that strong discharges would create more pores on the surface and increase the coating thickness [15,25].

The elemental composition of the PEO coatings were detected by EDS and the results are summarized in Table 1.

Table 1. Elemental composition of the PEO-coated samples determined from the EDS analysis

Electrolyte	Current density	Time (min)	Mg(wt%)	O(wt%)	Al(wt%)	Si(wt%)	C(wt%)
Without SiC nanoparticles	11.5 mA/cm^2	5	19.59	61.38	11.32	7.71	-
		10	25.45	45.32	17.91	11.32	-
		15	9.94	79.38	6.06	4.61	-
		20	6.74	85.64	4.29	3.34	-
	23 mA/cm^2	5	25.21	44.62	17.98	12.19	-
		10	7.03	84.46	4.90	3.61	-
		15	16.33	64.35	10.85	8.47	-
		20	7.37	83.92	4.81	3.9	-
With SiC nanoparticles	11.5 mA/cm^2	5	49.3	20.6	12	7.8	10.3
		10	34.5	25.3	14.2	13.1	12.9
		15	33.6	27.5	13.0	14.0	11.9
		20	41.2	23.6	13.2	23.7	17.5
	23 mA/cm^2	5	34.4	22.6	13.4	13.4	16.3
		10	25.8	19.8	13.2	23.7	17.5
		15	24.1	24.6	13.3	22.9	15.1
		20	22.8	21.1	13.1	26.1	16.9

EDS analysis reveal the presence of Mg and O as the major elements of the coatings. Other elements from the substrate and electrolyte including Al and Si were also found. As can be seen, a longer treatment time and higher current densities lead to an increase of Si:Mg and Al:Mg ratios.

According to the chemical and electrochemical bases, the following formation mechanism is proposed. These reactions can take place under cathodic and anodic conditions in the vicinity of the substrate. Previous investigations have shown that the major phases produced in aluminate and silicate based electrolytes are Mg_2SiO_4, MgO and $MgAl_2O_4$ [26]. During the first stages of the PEO process, Mg transforms into Mg^{2+} ion and then reacts with other ions present in the discharge channels such as O^{2-}, SiO_3^{2-}, OH^- and AlO^{2-}, which are obtained from the components of the electrolyte. MgO is formed by outward migration of Mg^{2+} ions from the anode (substrate) into the discharge channels and inward migration of O^{2-} ions form the electrolyte into the discharge channels because of the presence of high electric fields between the two poles of the cell [27,28].

$Mg \rightarrow Mg^{+2} + 2e-$ Eq.2

$Mg^{2+} + O^{2-} \rightarrow MgO$ Eq.3

Magnesium orthosilicate can be formed in two ways, according to equations 3 to 5 [28-30]:

$SiO_3^{2-} - 2e^- \rightarrow SiO_2 + ½\ O_2$ Eq.4

$2MgO + SiO_2 \rightarrow Mg_2SiO_4$ Eq.5

$2\ Mg^{2+} + 2\ SiO_3^{2-} \rightarrow Mg_2SiO_4 + SiO_2$ Eq.6

$MgAl_2O_4$ can also be formed via the following reactions [31]:

$AlO_2^- + 2H_2O \rightarrow Al(OH)_4^-$ Eq.7

$4\ Al(OH)_4^- - 4e^- \rightarrow 4Al(OH)_3 + 2H_2O + O_2$ Eq.8

$2Al(OH)_3 \rightarrow Al_2O_3 + 3H_2O$ Eq.9

$Mg^{2+} + 2\ Al(OH)_4^- \rightarrow MgAl_2O_4 + 4H_2O$ Eq.10

$Al_2O_3 + MgO \rightarrow MgAl_2O_4$ Eq.11

$Mg^{2+} + Al_2O_3 + 2OH^- \rightarrow MgAl_2O_4 + H_2O$ Eq.12

3.3. Hardness and wear properties of the PEO coatings

The microhardness of the Mg alloy substrate and PEO coatings prepared from two types electrolytes in different conditions are shown in Fig.7.

The hardness of the bare AZ31 Mg alloy is only about 64 HV. It can be seen that the microhardness of the oxide coatings is two to seven times higher than that of the magnesium alloy

substrate. The hardness of the coatings formed at short processing time is lower than that of coatings formed at longer processing times.

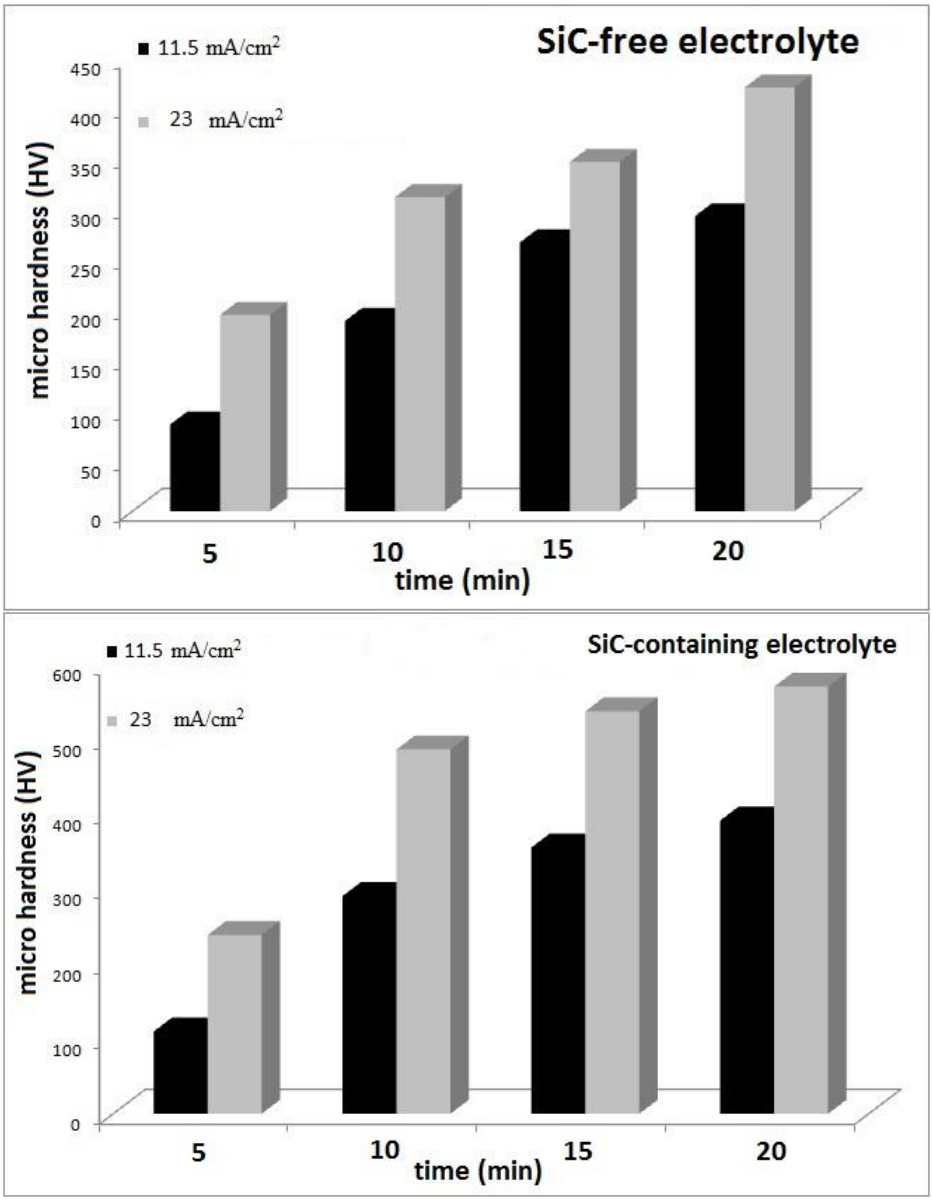

Figure 7. Vickers hardness of the oxide coatings obtained in different electrolytes and processing conditions.

The difference of micro-hardness of the PEO coatings can be mainly attributed to their composition. Observations showed that the micro-hardness of spinel Mg_2SiO_4 is higher than that of MgO [16,32]. Moreover, the content of Mg_2SiO_4 increases with increasing current density and processing time [15]. Furthermore, the microhardness of the samples processed in the electrolyte with SiC nanoparticles is higher than that of the coatings obtained from the electrolyte without SiC nanoparticles under the same processing parameters. It has been shown that the nanoparticles could fill

the pores or be embedded in the oxide coatings, leading to an increase the hardness of the coatings [24,33].

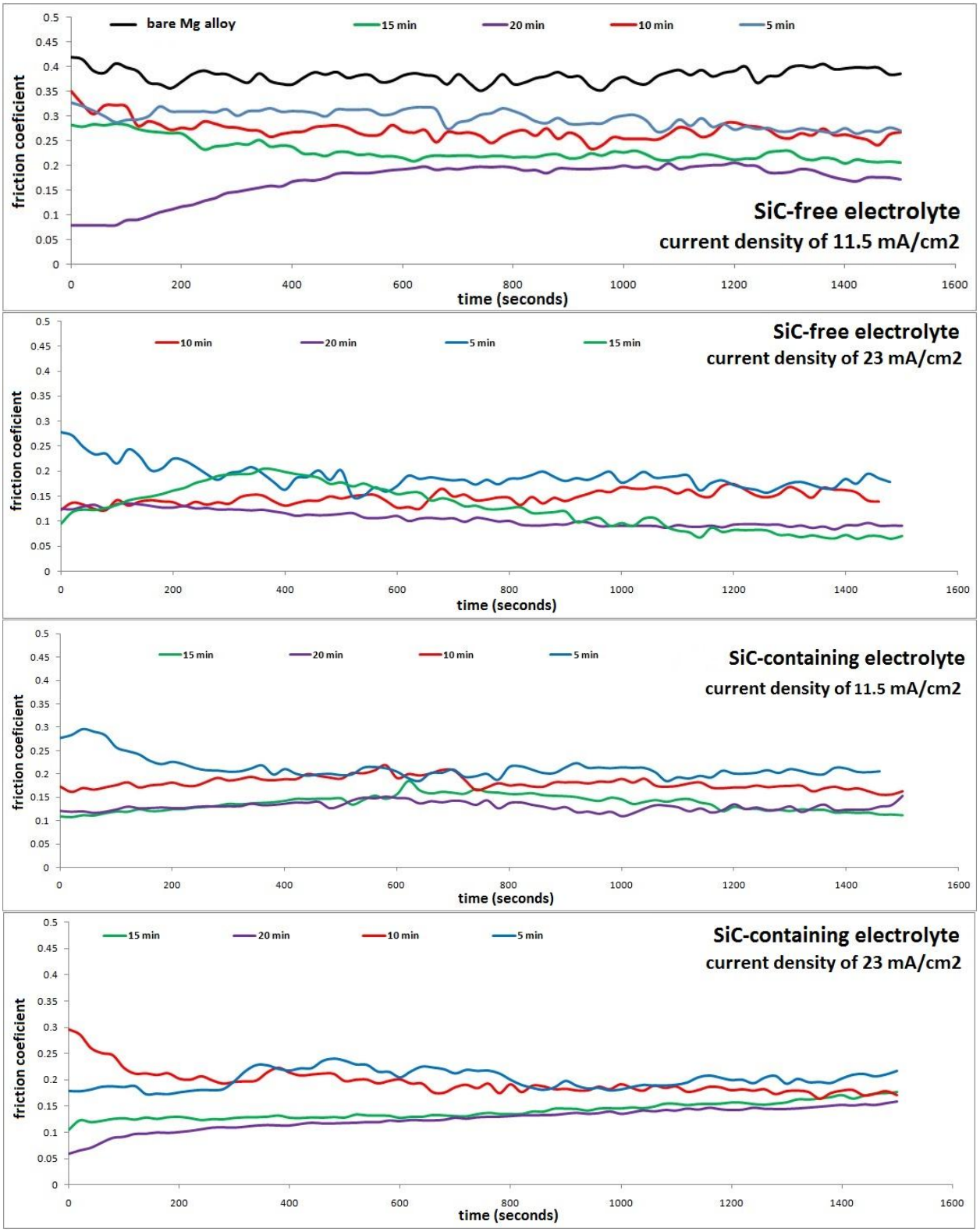

Figure 8. The relationship between the friction coefficients and testing time of various samples under dry sliding conditions.

The evolution of the friction coefficients versus sliding time for the PEO coatings is depicted in Fig.8. In addition, the friction coefficient of the uncoated substrate is also presented for comparison. As can be seen, compared with the uncoated substrate, all of the PEO-coated samples register lower friction coefficients under dry sliding conditions. It is also observed, there exist non-steady wear period in the wear process of the un-coated AZ31 magnesium alloy. The addition of SiC nanoparticles to the electrolyte results in obtaining nanocomposite coatings with lower and more stable friction coefficients than those prepared in SiC-free electrolyte. This may be due to the "rolling effect" made by SiC nanoparticles on the surface of the PEO coatings which acted as lubricants during the sliding tests [34].

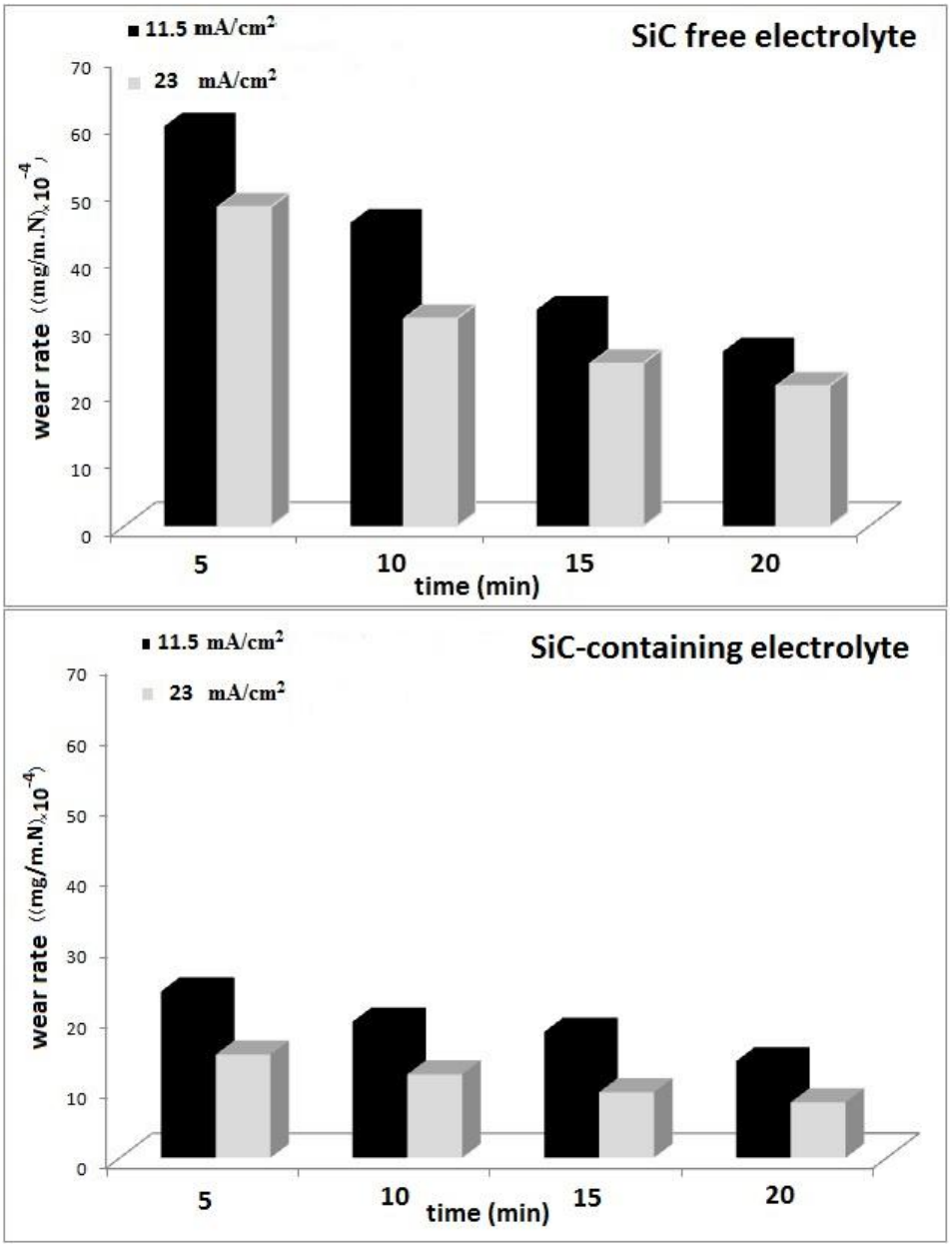

Figure 9. Wear rates obtained by pin-on-disc tests for the uncoated substrate and the PEO-Coated samples.

The wear rates of the PEO-coated samples were calculated, and results are shown in Fig.9. It can be seen that the wear rates of the SiC-containing PEO coatings are much smaller than the ordinary oxide coatings. Since the nanocomposite coatings get rolling friction and presence of the SiC nanoparticles increase the hardness of the coatings [35]. In the case of the wear mechanism of the nanocomposite coating, SiC nanoparticles lubricate as balls between the contact areas and hence change frictional form from sliding to rolling. This phenomenon results in the decrease of friction coefficient and also wear rate.

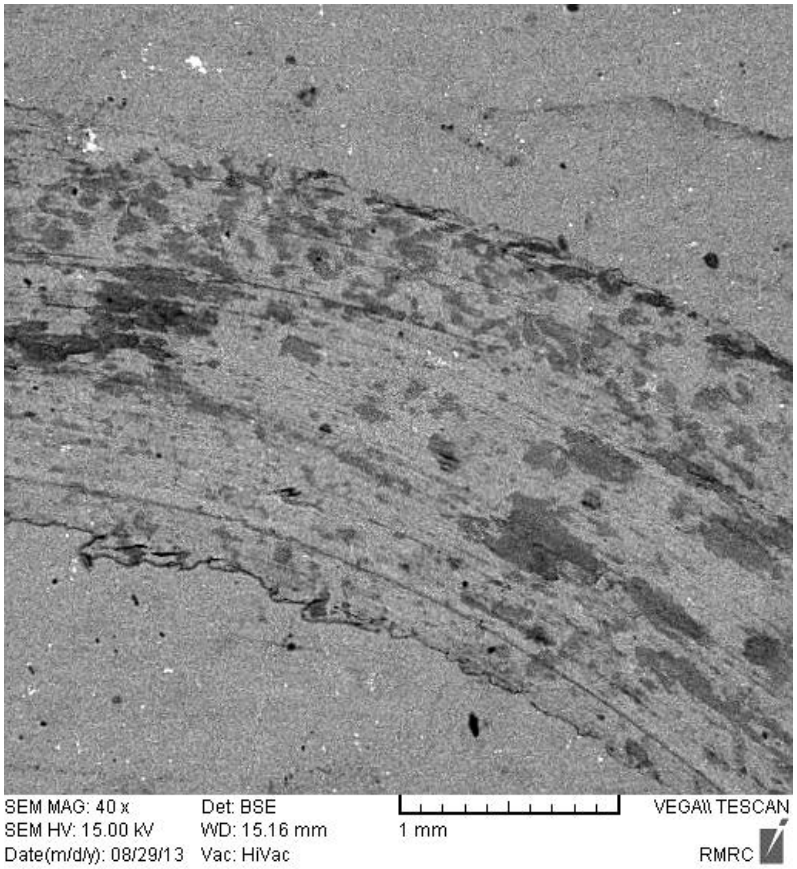

Figure 10. SEM micrograph of wear track of the bare Mg alloy.

The differences in the friction behavior and the wear rate of the PEO coatings have further been investigated by SEM micrographs of wear tracks, as shown in Fig.11. The SEM micrograph of wear track of the bare Mg alloy was also presented in Fig.10. It can be seen that the wear track of the un-coated magnesium alloy is deeper and wider than those of the PEO-synthesized coatings under the same wear conditions. There are wide ploughs and grooves on the worn surface of the bare magnesium alloy, indicating severe wear occurred on this sample. Investigations have shown that these characteristics of the worn surface represent the abrasive wear [24,36]. For the oxide coatings without SiC nanoparticles, relatively slight grooves and ploughs are seen and the widths of wear tracks become narrower and smother than the bare magnesium alloy because of their high hardness and load-bearing capacity.

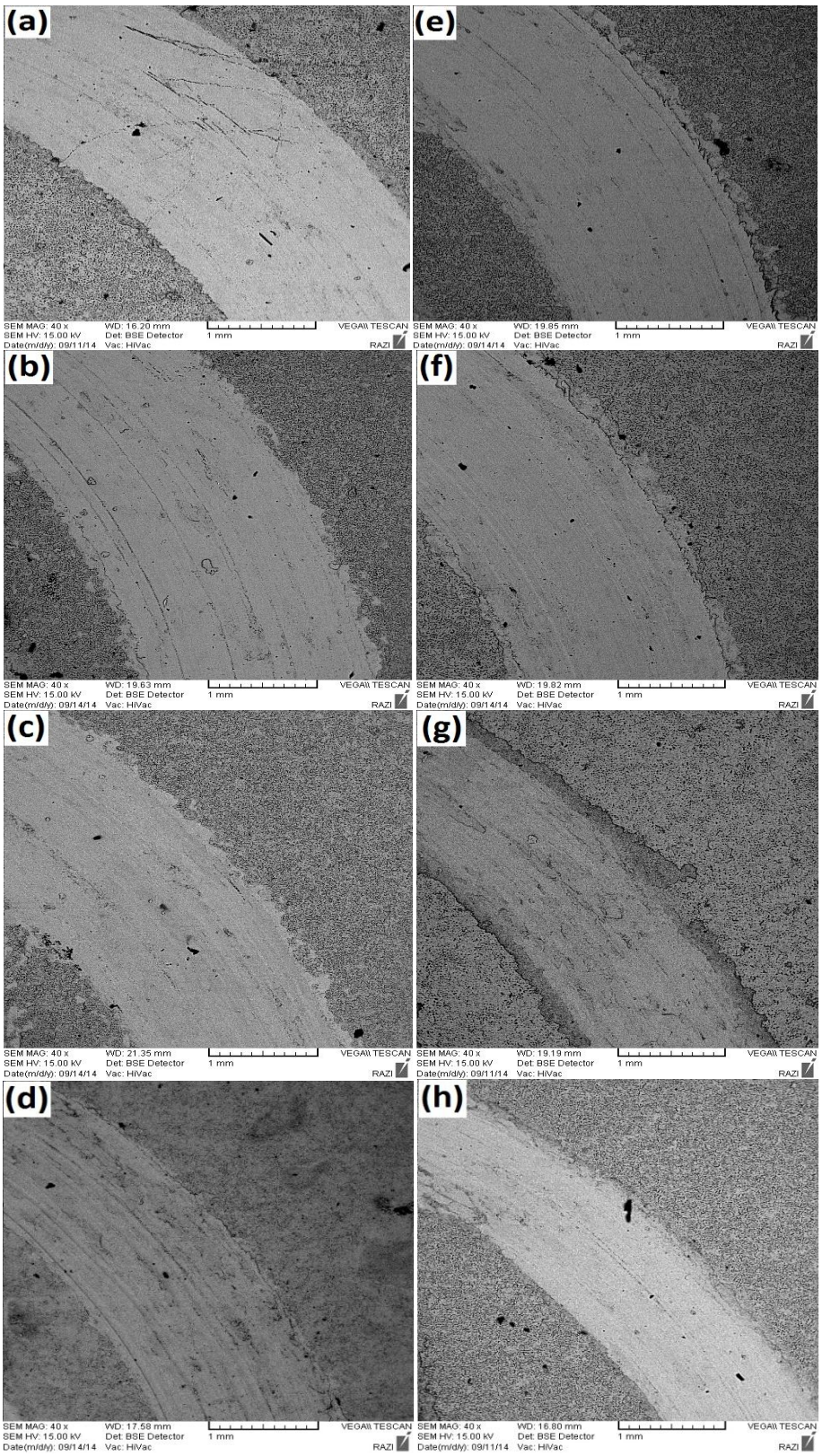

Figure 11. Wear track of PEO-synthesized coatings obtained in SiC-free electrolyte in current density of 11.5 mA/cm^2 (a-d) and 23 mA/cm^2 (e-h) at different time intervals of 5 min (a,e), 10 min (b,f), 15 min (c,g) and 20 min (d,f).

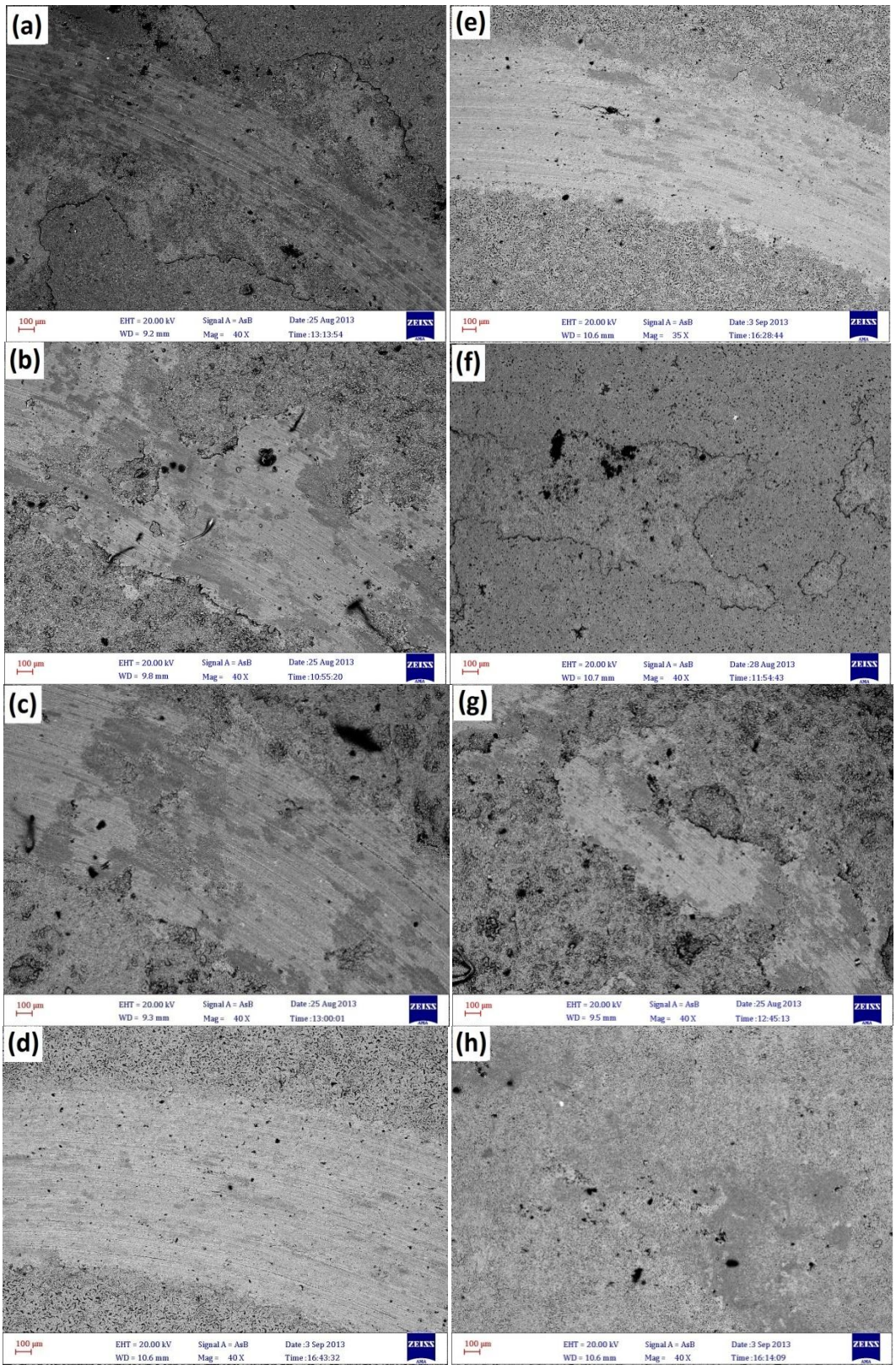

Figure 12. Wear track of PEO-synthesized coatings obtained in SiC-containing electrolyte in current density of 11.5 mA/cm^2 (a-d) and 23 mA/cm^2 (e-h) at different time intervals of 5 min (a,e), 10 min (b,f), 15 min (c,g) and 20 min (d,f).

Fig.12 shows the SEM morphologies of worn surfaces of the SiC-containing PEO coatings. The entire worn surfaces are quite smooth and no evidence of significant detachment of the coatings can be found. These observations indicate that only slight wear damage occurred on the surface of the nanocomposite coatings during sliding test.

It has been shown that the wear resistance of a sample has much to do with its surface hardness [37]. SiC is a kind of ultra hard particles and its hardness can be reach to HV 3000. When these nano-sized ceramic particles embedded into the coatings, even in a very low volume fraction, they can play a protective role in enhancing the wear resistance. These SiC nanoparticles distributed on the surface of the oxide coatings and then involved in the wear process during the sliding test. These particles reduce significantly the frictional shear stress between the coating and steel balls and leads to the decrease of the frictional coefficient and wear rate of the PEO coatings.

3.4. Electrochemical behavior of the PEO coatings

The corrosion resistance properties of the PEO coatings have been investigated using the effective electrochemical methods of potentiodynamic polarization technique and EIS in 3.5 wt.% NaCl solution.

3.4.1. Potentiodynamic polarization

The potentiodynamic polarization curves of the PEO coatings are shown in Fig.13. Corrosion current density (i_{corr}), corrosion potential (E_{corr}), cathodic and anodic Tafel slopes (b_c and b_a) were directly derived from these curves and the obtained data are summarized in Table 2.

Table 2. Corrosion-related parameters obtained from potentiodynamic polarization curves of Fig.13

Electrolyte	Current density	Time (min)	E_{corr} (mV)	I_{corr} (μA)	β_a (V/decade)	β_c (V/decade)	R_p ($\Omega.cm^2$)	mpy
Bare	-	-	-1505	32.74	85	321	175	150. 7
		5	-1478	9.25	72	201	489	42.6
	11.5	10	-1470	7.44	73	198	611	34.2
	mA/cm^2	15	-1463	2.53	10	87	332	11.6
Without SiC		20	-1485	1.84	190	107	3171	8.5
nanoparticles		5	-1491	7.73	48	182	419	35.6
	23	10	-1438	5.27	70	197	835	24.3
	mA/cm^2	15	-1499	1.98	91	87	1915	2.24
		20	-1515	0.89	235	192	10122	1.98
		5	-1486	7.22	85	152	644	33.2
	11.5	10	-1478	3.52	72	182	1249	16.2
	mA/cm^2	15	-1466	2.03	37	91	1105	9.4
With SiC		20	-1420	1.26	48	241	2708	5.8
nanoparticles		5	-1466	6.96	77	193	674	32.0
	23	10	-1418	1.81	98	196	3077	8.3
	mA/cm^2	15	-1475	2.70	215	256	3690	12.4
		20	-1470	0.13	33	64	13956	0.6

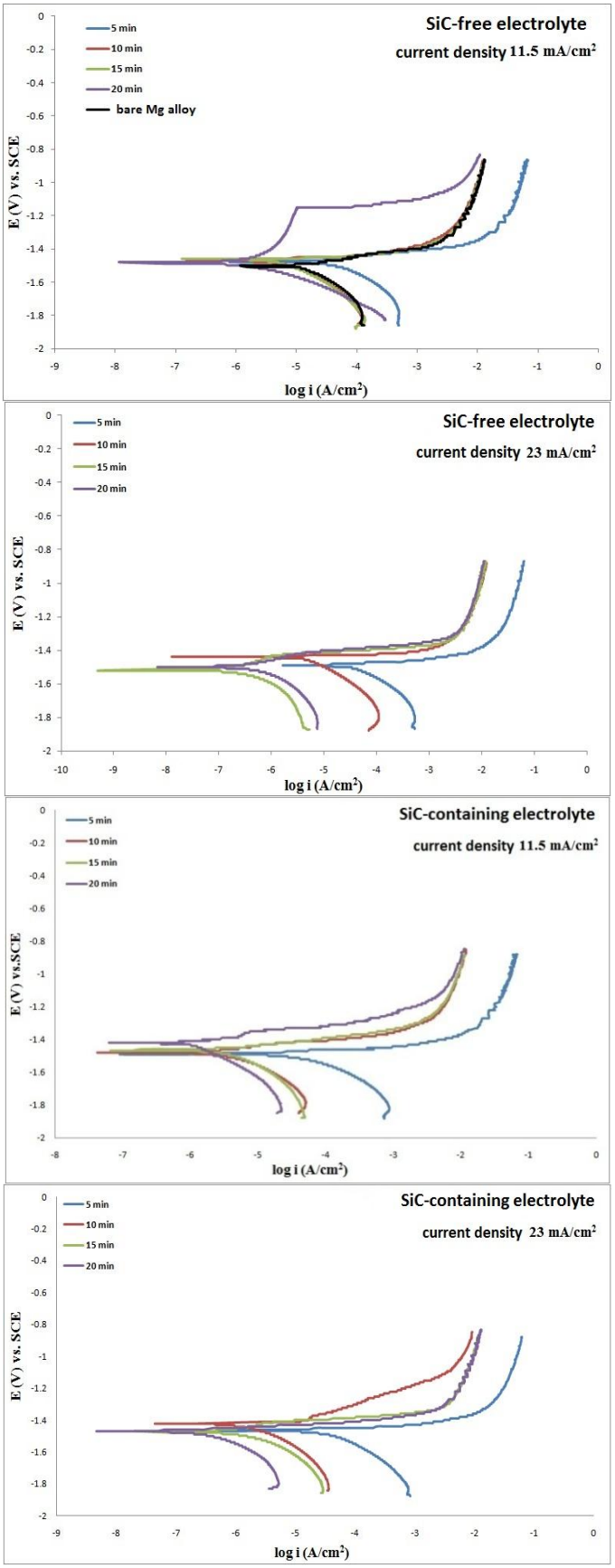

Figure 13. Potentiodynamic polarization curves of bare Mg alloy and PEO-coated samples in 3.5 wt.% NaCl aqueous solution at room temperature and open to air.

The polarization behavior of the bare magnesium alloy is also presented for comparison. According to the approximately linear polarization behavior near OCP, the polarization resistance (R_p) values were determined from Stern-Geary equation [38]:

$$R_p = \frac{b_a b_c}{2.303\, i_{corr}\,(b_a + b_c)} \qquad \text{Eq.13}$$

In a polarization curve, lower corrosion current density, higher polarization resistance and lower corrosion rate corresponds to better corrosion resistance of the sample. The results clearly show that the corrosion resistance of the magnesium alloy substrate was enhanced to a great extent when treated with PEO process. Furthermore, it is evident that the samples with nanocomposite coatings have even lower corrosion current densities than that of the coatings prepared in the SiC-free electrolyte. With the increase in the treatment time and current density, the corrosion current density tended to be lower.

The different polarization behavior of the samples coated in electrolytes with and without presence of SiC nanoparticles is mainly due to their different structure and composition. There are many micro pores and micro cracks on the surface of the PEO coatings (Figs.3 and 4) that are easy paths for transferring of corrosive intermediates (like Cl^- ions) into the inner layers of the coatings. This leads to increasing of polarization current density. In the case of the nanocomposite coatings, because of the blocking effect of the SiC nanoparticles (which deposited in the pores), transfer of Cl^- corrosive ions were held back and the increase of corrosion current density was suppressed during polarization measurements. Furthermore, SiC nanoparticles have poor electrical conductivity and hence they do not take part in electrochemical processes but rather cause hindrance [37]. Other reasons for better anti-corrosion behavior of the samples treated at longer processing times and higher current densities are their thicker PEO coatings and as well as higher amount of Mg_2SiO_4 and $MgAl_2O_4$, which have corrosion-resistance properties [32].

3.4.2. EIS

In order to further understand the anti-corrosion properties of the PEO coatings, EIS measurements in 3.5 wt.% NaCl solution were also done, and the resultant Niquest plots are shown in Fig.14.

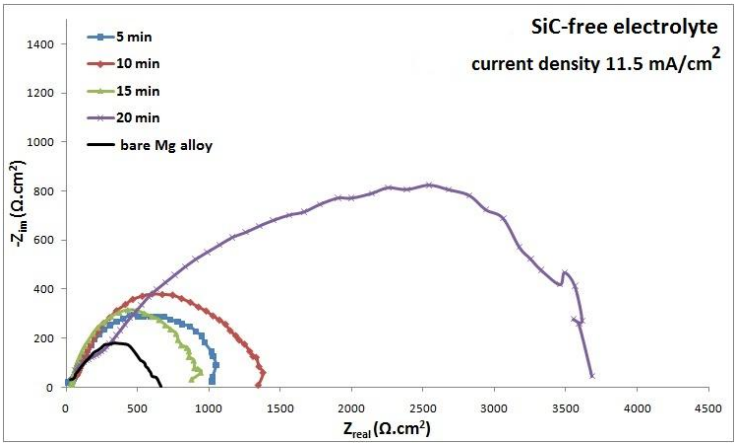

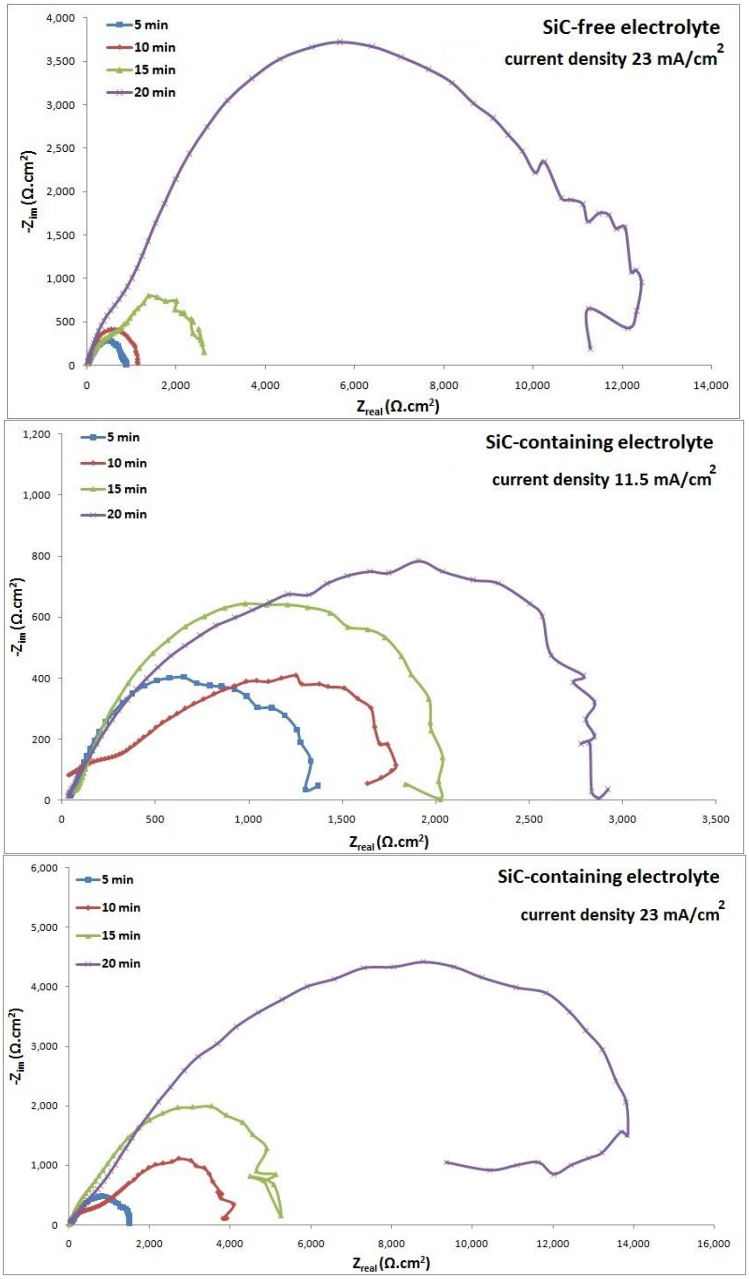

Figure 14. Niquest plots of uncoated and PEO-coated magnesium alloy AZ31 in 3.5 wt.% NaCl solution at room temperature and open to air after an immersion time of 1 h for stabilization.

The EIS results seem to confirm clearly the potentiodynamic polarization results. Corrosion resistance of the coatings depends on three factors: composition, structure and thickness. Because $MgAl_2O_4$ and Mg_2SiO_4 have higher stability in neutral environments than MgO, the increase in relative amount of these two phases in longer treatment times and higher current density will be beneficial to improving the corrosion resistance. In addition, thicker coatings can also contributed to better corrosion resistance for the samples prepared in higher current density and longer treatment times. The third factor influencing the corrosion resistance of the coatings is their surface morphology, specially pore density and size. According to the results, it can be concluded that the positive effect of the two

former factors overcome on the negative effect of the third factor. So, the corrosion resistance of the PEO-synthesized coatings was improved by increasing current density and treatment time.

4. CONCLUSIONS

Oxide coatings were formed on AZ31 magnesium alloy by plasma electrolytic oxidation in aluminate-silicate based electrolyte containing SiC nanoparticles in different constant current densities and time intervals. Different process parameters lead to differences in the structural characteristics of the obtained coatings, and subsequently cause the differences in the wear and corrosion behavior of the PEO coatings.

PEO coatings formed in SiC-containing electrolyte have higher microhardness than those formed in nanoparticle-free electrolyte. Under dry sliding conditions, the wear rate of the former are lower than that of the latter. Furthermore, the nanocomposite coatings exhibit a lower friction coefficient than those obtained in the electrolyte without SiC nanoparticles. The reason is that the SiC nanoparticles work as balls between the contact areas and then turn sliding friction to rolling friction.

Due to the blocking effect of the SiC nanoparticles, the nanocomposite coatings have much better corrosion resistance than the simple PEO coatings such as corrosion current density decreases and impedance also increases in 3.5 wt.% NaCl solution. Apart from pore plugging, the poor electrical conductivity of the SiC nanoparticles helps to enhancing anti-corrosion properties.

References

1. F. Muhaffel, F. Mert, H. Cimenoglu, D. Hoche, M.L. Zheludkevich, C. Blawert, *Surf. Coat. Technol.*, 269 (2015) 200.
2. J. Liang, P. Bala Srinivasan, C. Blawert, M. Stormer, W. Dietzel, *Electrochim. Acta*, 54 (2009) 3842.
3. G. Song, A. Atrens, D. St. John, X. Wu, J. Nairn, *Corros. Sci.*, 39 (1997) 1981.
4. N. Yamauchi, K. Demizu, N. Ueda, N.K. Cuong, T. Sone, Y. Hirose, *Surf. Coat. Technol.*, 193 (2005) 277.
5. L. White, Y. Koo, Y. Yun, J. Sankar, *J. Nanomaterials*, 2013 (2013) 15.
6. A.L. Yerokhin, X. Nie, A. Leyland, A. Matthews, S.J. Dowey, *Surf. Coat. Technol.*, 122 (1999) 73.
7. P. Gupta, G. Tenhundfeld, E.O. Daigle, D. Ryabkov, *Surf. Coat. Technol.*, 201 (2007) 8746.
8. S. Sarbishei, M.A. Faghihi Sani, M.R. Mohammadi, *Vacuum*, 108 (2014) 12.
9. V. Raj, M. Mubarak Ali, *J. Mater. Proces. Technol.*, 209 (2009) 5341.
10. L. Wang, L. Chen, Z. Yan, H. Wang, J. Peng, *J. Alloys Compd.*, 493 (2010) 445-452.
11. M. Laleh, A. Sabour Rouhaghdam, T. Shahrabi, A. Shanghi, *J. Alloys Compd.*, 496 (2010) 548.
12. R.H.U. Khan, A. Yerokhin, X. Li, H. Dong, A. Matthews, *Surf. Coat. Technol.*, 205 (2010) 1679.
13. S. Ikonopisov, *Electrochim. Acta*, 22 (1977) 1077.
14. J.M. Albella, I. Montero, J.M. Martı´nez-Duart, *Electrochim. Acta*, 32 (1987) 255.
15. Z. Li, Y. Yuan, X. Jing, *J. Alloys Compd.*, 541 (2012) 380.
16. J. Liang, L. Hu, J. Hao, *Appl. Surf. Sci.*, 253 (2007) 4490.
17. R. Arrabal, E. Matykina, F. Viejo, P. Skeldon, G.E. Thompson, M.C. Merino, *Appl. Surf. Sci.*, 254 (2008) 6937.
18. J. Liang, P.B. Srinivasan, C. Blawert, M. Störmer, W. Dietzel, *Appl. Surf. Sci.*, 255 (2009) 4212.

19. M.R. Bayati, F. Golestani-Fard, A.Z. Moshfegh, *Appl. Surf. Sci.*, 256 (2010) 4253.
20. F. Samanipour, M.R. Bayati, F. Golestani-Fard, H.R. Zargar, T. Troczynski, A.R. Mirhabibi, *Colloids surf. B*, 86 (2011) 14.
21. A. Rapacz-Kmita, A. Ślósarczyk, Z. Paszkiewicz, *J. Europ. Ceram. Soc.*, 26 (2006) 1481.
22. K.R. Shin, Y.S. Kim, G.W. Kim, Y.G. ko, D.H. Shin, *Colloids surf. B* , 131 (2015) 47.
23. A. Ghasemi, N. Scharnagl, C. Blawert, W. Dietzel, K.U. Kainer, *Surf. Eng.*, 26 (2010) 321.
24. D. Zhang, Y. Gou, Y. Liu, X. Guo, *Surf. Coat. Technol.* 236 (2013) 52.
25. A.L. Yerokhin, L.O. Snizhko, N.L. Gurevina, A. Leyland, A. Pilkington, A. Matthews, *J. Appl. Phys.*, 36 (2003), 2110.
26. S. Durdu, A. Aytac, M. Usta, *J. Alloys Compd.*, 509 (2011) 8601.
27. H.F. Guo, M.Z. An, H.B. Huo, S. Xu, L.J. Wu, *Appl. Surf. Sci.*, 252 (2006) 7911.
28. S. Durdu, M. Usta, *Appl. Surf. Sci.*, 261 (2012) 774-782.
29. S.G. Xin, L.X. Song, R.G. Zhao, X.F. Xu, *Mater. Chem. Phys.* 97 (2006) 132.
30. S.V. Gnedenkov, O.A. Khrisanfova, A.G. Zavidnaya, S.L. Sinebryukhov, V.S. Egorkin, M.V. Nistratova, A. Yerokhin, A. Matthews, *Surf. Coat. Technol.* 204 (2010) 2316.
31. H.F. Guo, M.Z. An, H.B. Huo, *Appl. Surf. Sci.*, 252 (2006) 7911.
32. Y. Wang, D. Wei, J. Yu, S. Di, *J. Mater. Sci. Technol.*, 30 (2014) 984.
33. M. Aliofkhazraei, A.S. Rouhaghdam, *Surf. Coat. Technol.*, 205 (2011) S57.
34. M. Mu, J. Liang, X. Zhou, Q. Xiao, *Surf. Coat. Technol.*, 214 (2013) 124.
35. S. Li, M. Zhu, J. Liu, M. Yu, L. Wu, J. Zhang, H. Liang, *Appl. Surf. Sci.*, 316 (2014) 28.
36. A.K. Mondal, B.S.S. Chandra, S. Kumar, *Tribol. Int.*, 40 (2007) 290.
37. L. Song-mei, Y. Xiu-mei, L. Jian-hua, Y. Mei, W. Liang, Y. Kang, *J. Cent. South Univ.*, 21 (2014) 4415.
38. M. Stern, A.L. Geary, *J. Electrochem. Soc.*, 104 (1957) 56.